

Probing flavor-diagonal couplings of doubly-charged scalar at low and high energies

Gang Li^{1,2,*} and Jin Sun^{3,†}

¹*School of Physics and Astronomy, Sun Yat-sen University, Zhuhai 519082, China*

²*Guangdong Provincial Key Laboratory of Quantum Metrology and Sensing, Sun Yat-Sen University, Zhuhai 519082, China*

³*Particle Theory and Cosmology Group, Center for Theoretical Physics of the Universe,
Institute for Basic Science (IBS), Daejeon 34126, Korea*

We investigate the phenomenology of a TeV-scale doubly-charged scalar from the right-handed sector within the framework of left-right symmetric models. Focusing on its flavor-diagonal couplings to right-handed electrons and muons, we assess probes from both high-energy colliders and low-energy precision experiments. High-energy processes include Bhabha scattering at LEP and future circular electron-positron colliders (CEPC/FCC-ee), direct production at the LHC, and dedicated searches and precision measurements at proposed muon colliders and μ TRISTAN. Low-energy observables encompass parity-violating Møller scattering, muon anomalous magnetic moment, and muonium–antimuonium oscillations. Our combined analysis indicates that for a doubly-charged scalar in the 1–3 TeV range, the flavor-diagonal Yukawa couplings to electrons and muons as small as 10^{-2} are accessible. Observations of such a doubly-charged scalar would potentially point toward the type-I seesaw mechanism of neutrino masses in the left-right symmetric model with D -parity breaking.

I. INTRODUCTION

The origin of neutrino masses remains one of the most profound open questions in particle physics. Explaining the tiny neutrino masses requires particles beyond the Standard Model (BSM). For example, in the type-I seesaw models [1–5], right-handed (RH) neutrinos are introduced, while in the type-II seesaw models [6–10], left-right symmetric models (LRSMs) [11–15], radiative neutrino mass models [10, 16, 17] and $d = 7$ neutrino mass models [18, 19] include one or more doubly-charged scalars. Seeking for new particles via their interactions with charged leptons thus paves one of the pathways towards verifying these scenarios.

In general, the Yukawa couplings of doubly-charged scalar are connected to neutrino masses and mixing, and contribute to charged lepton flavor violating (CLFV) processes. If the doubly-charged scalar is an $SU(2)$ singlet [10, 16, 17], it directly induces neutrino masses and lepton flavor mixing at the loop levels. If it arises from a scalar field in a higher $SU(2)$ representation, however, the Yukawa couplings of the doubly-charged scalar are the same as those of neutral component of the scalar field, which is responsible for generating neutrino masses and lepton flavor mixing. For example, in the minimal LRSM [4, 9], doubly-handed scalars emerge from the triplet scalars $\Delta_{L,R}$ after the spontaneous symmetry breaking of $SU(2)_L \times SU(2)_R \times U(1)_{B-L}$ gauge group. Since the left-right symmetry is explicitly imposed in the Yukawa sector, their couplings to leptons are equal and thus both severely constrained by the CLFV searches [20–22].

However, in non-manifest LRSMs, the RH Yukawa couplings of the doubly-charged scalar may differ from

those of the left-handed ones. In particular, in LRSMs with D -parity breaking [23, 24], parity and the $SU(2)_R$ breaking scale decouple, allowing the mass of RH doubly-charged scalar $\Delta_R^{\pm\pm}$ to be considerably smaller than the RH scale v_R . Within this LRSM framework, neutrino masses can be generated via either the type-I seesaw mechanism [24] or the type-II seesaw mechanism [25, 26].

Refs. [27, 28] investigated the sensitivities to the coupling of $\Delta_R^{\pm\pm}$ to electrons in both low- and high-energy processes, assuming a $\Delta_R^{\pm\pm}$ mass at the TeV scale, consistent with existing constraints from direct searches at the Large Hadron Collider (LHC). Recently, Ref. [29] proposed a concrete LRSM featuring a long-lived $\Delta_R^{\pm\pm}$. In this scenario, if the Yukawa couplings to charged leptons satisfy $|f_R| \lesssim 10^{-8}$, TeV-scale $\Delta_R^{\pm\pm}$ can decay outside the detector volume. Nevertheless, the magnitudes of $(f_R)_{\alpha\beta}$ are treated as being of the same order across different flavor indices α, β , so that the RH neutrino masses $M_R \sim f_R v_R$ are too small to generate light neutrino masses via the type-I seesaw mechanism, necessitating the introduction of additional fields [29].

In this work, we investigate the sensitivities to the RH Yukawa couplings $f_R^{\alpha\beta}$ for $\alpha, \beta = e, \mu$ in various low- and high-energy processes. Different from the parameter regions considered in Ref. [29], we focus on scenarios where the RH doubly-charged scalar $\Delta_R^{\pm\pm}$ resides at the TeV scale and decays promptly. We further assume that the flavor off-diagonal couplings are significantly suppressed relative to the flavor-diagonal ones, thereby satisfying stringent constraints from CLFV searches and allowing for sizable lepton-flavor-conserving coupling f_R^{ee} or $f_R^{\mu\mu}$. This assumption is justified since, light neutrino masses in the type-I seesaw mechanism are given by $M_\nu = -M_D M_R^{-1} M_D^T$, where the Dirac neutrino mass matrix M_D is generally complex. If future experiments observe no CLFV signals but detect signals in charged lepton-flavor-conserving processes, such observations could potentially point toward the RH doubly-charged scalar in

* ligang65@mail.sysu.edu.cn

† sunjin0810@ibs.re.kr (corresponding author)

non-manifest LRSMs, possibly the LRSM with D -parity breaking. For recent studies on a TeV-scale doubly-charged scalar focus on lepton-flavor-violating observables, see Refs. [30, 31].

The remainder of this paper is organized as follows. In Sec. II, we introduce the minimal model for the doubly-charged scalar that interacts with the leptons. We investigate the low-energy observables and high-energy processes that can probe the mass and Yukawa couplings of the doubly-charged scalar in Sec. III and Sec. IV, respectively. In Sec. V, we present the combined results and discuss their implications. We conclude in Sec. VI.

II. MINIMAL MODEL

We consider a minimal model motivated by the LRSM with D -parity breaking [23, 24] (see Ref. [29] for recent studies), which is based on the gauge group $SU(2)_L \times SU(2)_R \times U(1)_{B-L}$, with B and L being the baryon and lepton numbers, respectively. The relevant Yukawa interactions of triplet scalar to leptons are given by

$$\mathcal{L}_Y = -(\bar{L}_L^c i\tau_2 \Delta_L f_L L_L + \bar{L}_R^c i\tau_2 \Delta_R f_R L_R) + \text{h.c.}, \quad (1)$$

where the LH and RH lepton doublets are defined as

$$L_L = \begin{pmatrix} \nu_L \\ \ell_L \end{pmatrix}, \quad L_R = \begin{pmatrix} \nu_R \\ \ell_R \end{pmatrix}, \quad (2)$$

and the scalar triplets are

$$\Delta_{L,R} = \begin{pmatrix} \Delta_{L,R}^+/\sqrt{2} & \Delta_{L,R}^{++} \\ \Delta_{L,R}^0 & -\Delta_{L,R}^+/\sqrt{2} \end{pmatrix}. \quad (3)$$

In Eq. (1), τ_2 is the second Pauli matrix, $f_{L,R}$ represents the Yukawa coupling matrices, and $\bar{L}_{L,R}^c \equiv L_{L,R}^T C$ with C being the charge conjugation matrix, and “h.c.” denotes the Hermitian conjugate.

After electroweak symmetry breaking, the neutral components of $\Delta_{L,R}$ acquire vacuum expectation values (vevs), $\langle \Delta_{L,R}^0 \rangle = v_{L,R}/\sqrt{2}$. The masses of Δ_L are expected to be at the D -parity breaking scale, which lies significantly above the $SU(2)_R$ breaking scale [23, 24], thus Δ_L effectively decouples from the processes considered here. It was emphasized in Ref. [29] that the mass of the singly-charged scalar Δ_R^\pm must exceed 15 TeV to satisfy constraints from $K - \bar{K}$ and $B - \bar{B}$ mixings [32–35], whereas the mass of the doubly-charged scalar $\Delta_R^{\pm\pm}$ can be arbitrarily small. In addition, we assume that the vev v_R is sufficiently large, so that the RH gauge bosons are also irrelevant to our analysis, which focuses on $\Delta_R^{\pm\pm}$ in both low- and high-energy processes¹.

Furthermore, we assume the flavor off-diagonal Yukawa couplings $f_R^{\alpha\beta}$ with $\alpha \neq \beta$ are negligible, while

the diagonal couplings satisfy $|f_R^{\alpha\alpha}| \geq 10^{-3}$ for $\alpha = e, \mu$. Under this assumption, viable light neutrino masses and mixing can still be achieved in the type-I seesaw mechanism without the need of introducing additional singlet fermion fields, as required in Ref. [29]. This is possible because the RH neutrino masses $M_R \sim f_R v_R$ could have adequate magnitude, and the Dirac neutrino mass matrix M_D is a general complex matrix. For simplicity, we take the leptonic Yukawa couplings to be real and positive throughout this work.

III. LOW-ENERGY OBSERVABLES

In this section, we will investigate constraints on the mass and Yukawa couplings of $\Delta_R^{\pm\pm}$ using the low-energy observables, including parity-violating asymmetry in Møller scattering, muon anomalous magnetic moment, and muonium-antimuonium transition probability.

A. Møller scattering

It has been investigated in Refs. [27, 36] that the couplings of $\Delta_R^{\pm\pm}$ to the electrons can be probed in the Møller scattering ($e^-e^- \rightarrow e^-e^-$) process via the s -channel exchange of $\Delta_R^{\pm\pm}$. By using the Firez transformation, we derive the effective interaction at low energies as

$$\mathcal{L}_{\text{PV}} = \frac{(f_R^{ee})^2}{2m_{\Delta^{++}}^2} (\bar{e}_R \gamma^\mu e_R) (\bar{e}_R \gamma_\mu e_R), \quad (4)$$

where we have ignored the contribution from the left-handed doubly-charged scalar, and $m_{\Delta^{++}}$ represents the mass of the RH doubly-charged scalar $\Delta_R^{\pm\pm}$. The upcoming MOLLER experiment [37], which aims to measure the parity-violating asymmetry of the Møller scattering with unprecedented sensitivity, can put the following low bound

$$\frac{m_{\Delta^{++}}}{f_R^{ee}} > 7.6 \text{ TeV} \quad (5)$$

at 95% confidence level (C.L.) [28].

B. Muon $g - 2$

Given the coupling to muons $f_R^{\mu\mu}$, the doubly-charged scalar $\Delta_R^{\pm\pm}$ can contribute to the muon anomalous magnetic moment, i.e., $(g - 2)_\mu$, at one-loop level, which is expressed as [38–42]

$$\Delta a_\mu = -\frac{m_\mu^2}{24\pi^2} \frac{(f_R^{\mu\mu})^2}{m_{\Delta^{++}}^2}, \quad (6)$$

with m_μ being the muon mass. Based on the latest measurement of $(g - 2)_\mu$ by the FNAL experiment [43], and the updated SM prediction in lattice-QCD calcula-

¹ Consequently, we do not consider the searches for neutrinoless double beta decay. For a detailed study of the scenarios where W_R does not decouple, see Ref. [28].

tion [44], we obtain the difference

$$a_\mu^{\text{exp}} - a_\mu^{\text{SM}} = 39(64) \times 10^{-11}, \quad (7)$$

which can be negative at 1σ level. We thus obtain an upper bound on $f_R^{\mu\mu}/m_{\Delta^{++}} < 4.3 \text{ TeV}^{-1}$ at 2σ level from the $(g-2)_\mu$ measurement.

Similarly, the coupling of $\Delta_R^{\pm\pm}$ to electrons yields a negative contribution to the electron anomalous magnetic moment $(g-2)_e$. However, depending on whether the fine-structure constant is determined from rubidium [45] or cesium [46], the difference between the experimental value and the SM prediction currently shows a sign discrepancy [47]. It remains premature to draw definitive conclusions. Therefore, we do not include constraints from $(g-2)_e$ in this work.

C. Muonium-antimuonium transition

The muonium to antimuonium transition has recently drawn considerable attention both theoretically [48–53] and experimentally [54–56]. The muonium (dubbed M) is a bound state of μ^+ and e^- , thus this process can probe BSM physics that violates lepton flavor number by two units $\Delta L_\mu = -\Delta L_e = 2$ [48, 57, 58], which is not directly constrained by the CLFV searches with $\Delta L = 1$ [22].

Besides, $M - \bar{M}$ transition can also be induced by t -channel exchange of a doubly-charged scalar [49, 50, 59], without involving lepton flavor violation. At low energies, we obtain the following effective interaction [59, 60]

$$\mathcal{L}_{M-\bar{M}} = \frac{f_R^{ee} f_R^{\mu\mu}}{2m_{\Delta^{++}}^2} (\bar{\mu}_R \gamma^\mu e_R) (\bar{\mu}_R \gamma^\mu e_R). \quad (8)$$

Depending on the spin orientation, muonium can be produced in either the spin-0 or spin-1 state, referred to as para-muonium (M_P) and ortho-muonium (M_V), respectively. The total transition probability is a weighted sum of these two contributions [48]

$$P(M \rightarrow \bar{M}) = \sum_{i=P,V} f_i P(M_i \rightarrow \bar{M}_i), \quad (9)$$

where the fractions $f_P + f_V = 1$. Following Refs. [59, 61], we parameterize the transition probability of para-muonium as

$$\begin{aligned} P(M_P \rightarrow \bar{M}_P) &= 64^3 \left(\frac{3\pi^2 \alpha_{\text{em}}^3}{G_F m_\mu^2} \right)^2 \left(\frac{m_e}{m_\mu} \right)^6 \left(\frac{G_{M\bar{M}}}{G_F} \right)^2 \\ &= 2.64 \times 10^{-5} \left(\frac{G_{M\bar{M}}}{G_F} \right)^2, \end{aligned} \quad (10)$$

where α_{em} is the fine-structure constant, m_e is the electron mass, and G_F denotes the Fermi constant. The effective coupling is given by [48, 49, 59]

$$G_{M\bar{M}} = \frac{f_R^{ee} f_R^{\mu\mu}}{4\sqrt{2}m_{\Delta^{++}}^2}. \quad (11)$$

The transition probability of ortho-muonium is [48]

$$P(M_V \rightarrow \bar{M}_V) = 9P(M_P \rightarrow \bar{M}_P). \quad (12)$$

The most stringent constraint to date comes from the MACS experiment at PSI [62], which places an upper limit on the $M - \bar{M}$ transition probability of $P(M \rightarrow \bar{M}) < 8.3 \times 10^{-11}/S_B(B_0)$ at 90% confidence level (CL). The factor $S_B(B_0)$ accounts for the suppression of the transition due to the external magnetic field [63, 64]. For the MACS experiment, the magnetic field strength $B_0 = 0.1 \text{ T}$, leading to $S_B(B_0) = 0.35$ [62]. The proposed MACE experiment, operating at the same magnetic field strength, is expected to improve the sensitivity beyond the level of 10^{-13} [55]. From Ref. [50], we can effectively take $f_P = 1$ for the MACS experiment, and derive the upper bound $G_{M\bar{M}}/G_F < 3 \times 10^{-3}$. On the other hand, as in Ref. [55], we estimate the sensitivity of MACE by assuming $f_P = 0.3$, and obtain $G_{M\bar{M}}/G_F < 4 \times 10^{-5}$.

IV. HIGH-ENERGY PROCESSES

The doubly-charged scalar can also contribute to high-energy processes at hadron and lepton colliders. The most stringent constraint on the mass of the doubly-charged scalar $\Delta_R^{\pm\pm}$ arises from direct searches conducted at the LHC, specifically through their pair production in the Drell-Yan process $pp \rightarrow \Delta_R^{++} \Delta_R^{--}$. Each scalar decays into a pair of same-sign leptons. Based on the searches performed during LHC Run 2, which analyzed an integrated luminosity of 139 fb^{-1} , the mass range $m_{\Delta_R^{++}} < 1.08 \text{ TeV}$ has been excluded [65]. We adopt a conservative lower limit of $m_{\Delta_R^{++}} \geq 1.4 \text{ TeV}$, since the decay branching ratios of $\Delta_R^{\pm\pm}$ are different from those assumed in the experimental analysis.

On the other hand, bound on $f_R^{ee}/m_{\Delta^{++}}$ is set by Bhabha scattering $e^+e^- \rightarrow e^+e^-$ at the Large Electron-Positron Collider (LEP). Reinterpreting the combined LEP limit from data collected at DELPHI, ALEPH, and OPAL [66], which correspond to the mean center-of-mass energy $\sqrt{s} = 195.6 \text{ GeV}$ and a total integrated luminosity of $\mathcal{L} = 745 \text{ pb}^{-1}$ [67], we obtain [28, 68]

$$\frac{m_{\Delta^{++}}}{f_R^{ee}} > 2.43 \text{ TeV}. \quad (13)$$

It is evident that the current constraints on Yukawa couplings to leptons are relatively weak, particularly in light of the mass limits on the doubly-charged scalar established by direct searches at the LHC. In the below, we will examine the sensitivities of the processes illustrated in Fig. 1 to the ratio $f_R^{\alpha\alpha}/m_{\Delta^{++}}$ at future high-energy lepton colliders².

² Similar processes have been proposed long time ago [36] to search for doubly-charged scalars in the LRSM at e^+e^-/e^-e^- colliders.

- e^+e^- colliders: CEPC [69] and FCC-ee [70] with $\sqrt{s} = 240$ GeV and $\mathcal{L} = 5 \text{ ab}^{-1}$.
- $\mu^+\mu^-$ colliders: future muon colliders [71, 72] with $\sqrt{s} = 3$ TeV (10 TeV) and $\mathcal{L} = 1 \text{ ab}^{-1}$ (10 ab^{-1}).
- $\mu^+\mu^+$ collider: μ TRISTAN with $\sqrt{s} = 2$ TeV and $\mathcal{L} = 12 \text{ fb}^{-1}$ [73, 74].
- μ^+e^- collider: μ TRISTAN with $\sqrt{s} = 346$ GeV and $\mathcal{L} = 1 \text{ ab}^{-1}$ [73, 74].

The solid curves in Fig. 2 show the analytically computed cross sections versus $m_{\Delta^{++}}$ for the benchmark values $f_R^{ee} = f_R^{\mu\mu} = 0.1$. They are cross-checked with MADGRAPH5_AMC@NLO [75, 76] (dashed curves). The results agree well with each other.

For convenience, we separate the total cross section

$$\sigma_i = \sigma_i^{\text{SM}} + \sigma_i^{\text{NP}}, \quad (14)$$

where i represents the process under consideration, the terms with superscripts “SM” and “NP” denotes the contributions from the SM and doubly-charged scalar including its interference with the SM, respectively.

A. CEPC/FCC-ee

At future electron-positron colliders CEPC/FCC-ee [69, 70] with the center-of-mass energy $\sqrt{s} = 240$ GeV, Bhabha scattering is expected to be measured with higher precision than the LEP due to a larger number of signal events. In order to derive the sensitivities of CEPC/FCC-ee to $m_{\Delta^{++}}/f_R^{ee}$, we calculate the cross section of Bhabha scattering involving the contribution from $\Delta_R^{\pm\pm}$.

The Bhabha scattering $e^+e^- \rightarrow e^+e^-$ occurs via the s -channel and t -channel exchange of γ/Z in the SM. The doubly-charged scalar $\Delta_R^{\pm\pm}$ can contribute to this process in the u channel, as depicted in Fig. 1(a).

We obtain

$$\sigma_{e^+e^- \rightarrow e^+e^-}^{\text{NP}} = \frac{1}{16\pi s^2} \int_{t_{\min}}^{t_{\max}} dt [|\mathcal{M}_\Delta|^2 + \mathcal{M}_{\text{int}}^2], \quad (15)$$

where the squared amplitude for the exchange of $\Delta_R^{\pm\pm}$ and the term describing interference with the SM are expressed as

$$|\mathcal{M}_\Delta|^2 = \frac{(f_R^{ee})^4 u^2}{4[(u - m_{\Delta^{++}}^2)^2 + \Gamma_\Delta^2 m_{\Delta^{++}}^2]}, \quad (16)$$

$$\mathcal{M}_{\text{int}}^2 = \frac{e^2 (f_R^{ee})^2 u^2 [g(s) - g(t)]}{4[(u - m_{\Delta^{++}}^2)^2 + \Gamma_\Delta^2 m_{\Delta^{++}}^2]}. \quad (17)$$

Hereafter, the lepton masses are neglected. The function

$g(x)$ is defined as

$$g(x) = (u - m_{\Delta^{++}}^2) \left[\frac{4}{x} + \frac{(x - m_Z^2)}{4c_W^2 s_W^2 |D_Z(x)|^2} \right] + \frac{m_{\Delta^{++}} \Gamma_\Delta m_Z \Gamma_Z}{4c_W^2 s_W^2 |D_Z(x)|^2}, \quad (18)$$

with

$$D_Z(x) \equiv x - m_Z^2 + i\Gamma_Z m_Z. \quad (19)$$

In the above, Γ_Z and m_Z are the width and mass of Z boson, respectively, while Γ_Δ denotes the width of $\Delta_R^{\pm\pm}$. Besides, s , t and u are the Mandelstam variables. s_W and c_W denote the sine and cosine of the weak mixing angle, respectively.

The variable t is a monotonic function of the pseudo-rapidity η ,

$$t = -\frac{s}{1 + e^{2\eta}}, \quad \eta \equiv -\ln \tan(\theta/2). \quad (20)$$

In experimental searches, cut on the rapidity $|\eta| < \eta_{\text{cut}}$ should be imposed, which leads to

$$t_{\min} = -\frac{s}{1 + e^{-2\eta_m}} \quad t_{\max} = -\frac{s}{1 + e^{2\eta_m}}. \quad (21)$$

The measured cross section at LEP [66] required the average polar scattering angle to satisfy $|\cos \theta| < 0.90$ ($|\eta| < 1.47$). In contrast, detectors at future circular colliders like CEPC/FCC-ee can cover a larger angular range. In practice, we take $|\cos \theta| < 0.9998$ ($|\eta| < 4.56$) based on Ref. [77] for the studies CEPC/FCC-ee [69, 70].

The purple curve in Fig. 2 shows the total cross section $\sigma_{e^+e^- \rightarrow e^+e^-}$ for Bhabha scattering at CEPC/FCC-ee for $f_R^{ee} = 0.1$. This cross section is larger than that at LEP. The increase occurs because the differential cross section peaks in the forward direction ($|\cos \theta| \rightarrow 1$). The CEPC/FCC-ee’s enhanced angular acceptance captures more of these forward events. This compensates for the kinematic suppression from the higher center-of-mass energy and results in a larger total cross section.

Besides, we can see that the cross section only has a mild dependence on $m_{\Delta^{++}}$. For example, for $m_{\Delta^{++}} = 1.4$ TeV, we obtain $\sigma_{e^+e^- \rightarrow e^+e^-}^{\text{NP}} / \sigma_{e^+e^- \rightarrow e^+e^-}^{\text{SM}} = -7 \times 10^{-7}$. It indicates that interference with the SM is destructive and $\sigma_{e^+e^- \rightarrow e^+e^-}^{\text{NP}}$ approximately scales with $(f_R^{ee}/m_{\Delta^{++}})^2$.

To evaluate the sensitivity, we derive the exclusion at 95% confidence level (CL) using the following criterion

$$\frac{n_s}{\sqrt{n_s + n_b}} \geq 1.96. \quad (22)$$

For the Bhabha scattering at CEPC/FCC-ee, the numbers of events are given by

$$n_s = -\sigma_{e^+e^- \rightarrow e^+e^-}^{\text{NP}} \mathcal{L}, \quad n_b = \sigma_{e^+e^- \rightarrow e^+e^-}^{\text{SM}} \mathcal{L}, \quad (23)$$

and the integrated luminosity $\mathcal{L} = 5 \text{ ab}^{-1}$. The resulting exclusion limits for different $m_{\Delta^{++}}$ are shown in purple in Fig. (3,4).

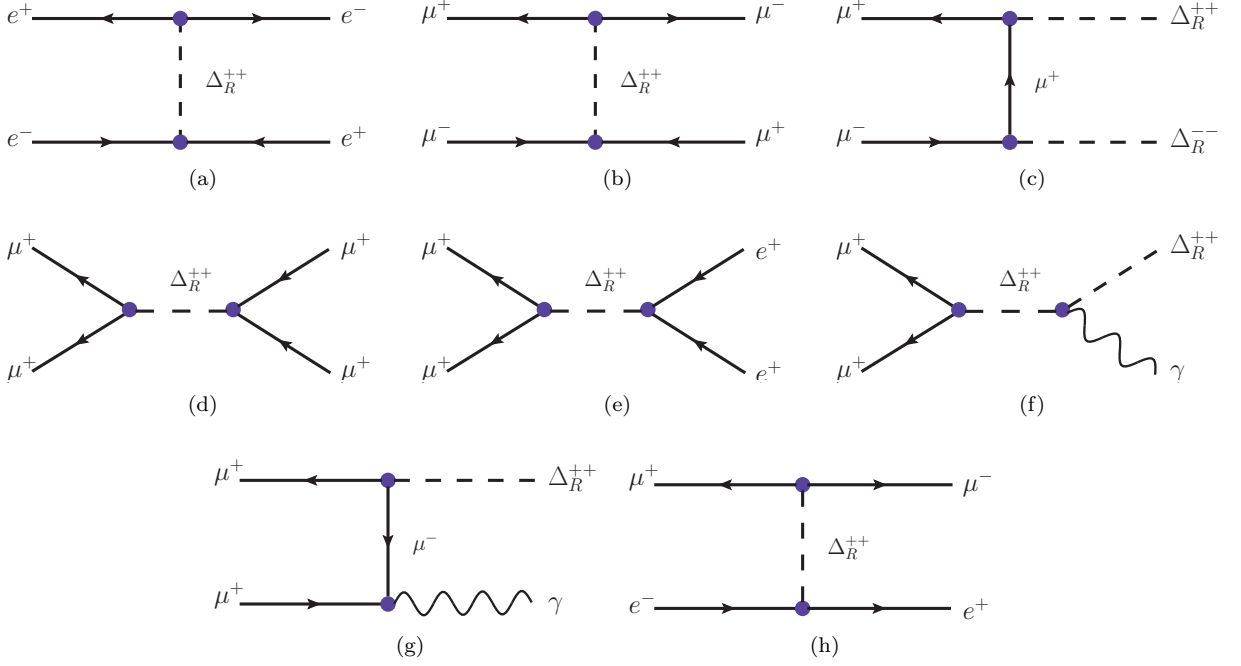


Figure 1: Representative Feynman diagrams for the high-energy processes with the exchange or production of $\Delta_R^{\pm\pm}$.

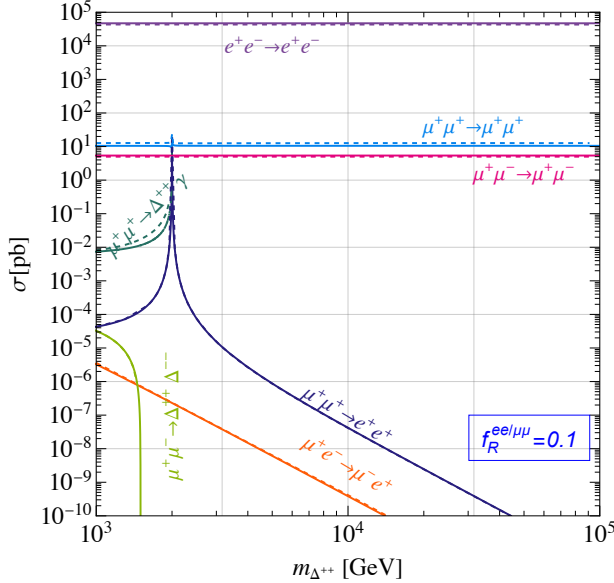


Figure 2: Total cross section as a function of $m_{\Delta^{++}}$ for various processes at different colliders: e^+e^- ($\sqrt{s} = 240$ GeV), $\mu^+\mu^-$ ($\sqrt{s} = 3$ TeV), $\mu^+\mu^+$ ($\sqrt{s} = 2$ TeV), and μ^+e^- ($\sqrt{s} = 346$ GeV). Analytical results are shown as solid lines; cross-checks from MADGRAPH5_AMC@NLO are shown as dashed lines.

In addition to the total cross section, the analysis can be performed using differential distributions, as was done at LEP. To estimate the sensitivity, we

rescale the existing limit on $f_R^{ee}/m_{\Delta^{++}}$ by a factor of $\sqrt{(\sigma_{\text{LEP}}\mathcal{L}_{\text{LEP}})/(\sigma_{e^+e^-}\mathcal{L}_{e^+e^-})}$, following Refs. [27, 28]. Here, σ_{LEP} and $\sigma_{e^+e^-}$ denote the magnitudes of the NP contributions to the Bhabha scattering at LEP and CEPC/FCC-ee, respectively. The integrated luminosities are $\mathcal{L}_{\text{LEP}} = 745 \text{ pb}^{-1}$ and $\mathcal{L}_{e^+e^-} = 5 \text{ ab}^{-1}$.

B. Muon colliders

Given the current bound on the mass of $\Delta_R^{\pm\pm}$, we consider the future muon collider (MuC) with the center-of-mass energy $\sqrt{s} = 3$ TeV (10 TeV) [71, 72], which provides opportunities for both precision tests of the process $\mu^+\mu^- \rightarrow \mu^+\mu^-$, and direct production of on-shell doubly-charged scalars via $\mu^+\mu^- \rightarrow \Delta_R^{++}\Delta_R^{--}$, which are shown in Fig. 1(b) and Fig. 1(c), respectively.

For the process $\mu^+\mu^- \rightarrow \mu^+\mu^-$, the expression of cross section is the same as that for the Bhabha scattering, with the substitution of e to μ . The benchmark cross section is shown in Fig. 2. We consider the integrated luminosity $\mathcal{L} = 1 \text{ ab}^{-1}$ (10 ab^{-1}) for 3 TeV (10 TeV) MuC, and baseline cut on the pseudo-rapidity of leptons $|\eta| < 2.5$ [72]. The constraint on $f_R^{\mu\mu}/m_{\Delta^{++}}$ is obtained from the precise measurement of the cross section for the process $\mu^+\mu^- \rightarrow \mu^+\mu^-$ with the exclusion limits derived using Eq. (22).

Besides, the pair production process $\mu^+\mu^- \rightarrow \Delta_R^{++}\Delta_R^{--}$ is possible if the center-of-mass energy $\sqrt{s} >$

$2m_{\Delta^{++}}$. The cross section is given by

$$\sigma_{\mu^+\mu^-\rightarrow\Delta_R^{++}\Delta_R^{--}} = \frac{(f_R^{\mu\mu})^4(s-2m_{\Delta^{++}}^2)}{64\pi s^2} \ln \frac{w_+}{w_-} - \frac{(f_R^{\mu\mu})^4 \sqrt{s(s-4m_{\Delta^{++}}^2)}}{32\pi s^2}, \quad (24)$$

with $w_{\pm} \equiv s - 2m_{\Delta^{++}}^2 \pm \sqrt{s(s-4m_{\Delta^{++}}^2)}$. The on-shell $\Delta_R^{\pm\pm}$ can subsequently decay into a pair of same-sign leptons with the same flavor. The partial decay width of $\Delta_R^{++} \rightarrow \ell^+\ell^+$, where $\ell = e, \mu$, is given by

$$\Gamma_{\ell\ell} = \frac{(f_R^{\ell\ell})^2 m_{\Delta^{++}}}{4\pi} \sqrt{1 - \frac{m_{\ell}^2}{m_{\Delta^{++}}^2}}. \quad (25)$$

Since the sensitivity to the Yukawa couplings depends on the flavor combination of the two decay chains, we consider three distinct cases: $4e$, 4μ , and $2e2\mu$. From the collider simulation in Ref. [78], these final states are nearly background free, and the signal efficiencies are about 50% – 80%. We assume a conservative and universal signal efficiency of 50%, and derive the 95% CL exclusion limits by requiring at least 3 signal events assuming no SM background [79, 80]. The results for 3 TeV and 10 TeV MCs are presented in Fig. 3 and Fig. 4, respectively.

C. μ TRISTAN

By utilizing a low-emittance muon beam originally developed for the measurements of muon $g-2$ at J-PARC [81], a new collider design known as μ TRISTAN has been proposed [73]. By accelerating μ^+ and e^- beams up to 1 TeV and 30 GeV, respectively, the center-of-mass energies of 2 TeV and 346 GeV can be achieved for colliding $\mu^+\mu^+$ and μ^+e^- , respectively. At both colliders, lepton number violation (LNV) can be probed through same-sign dilepton signals arising from the Yukawa interactions given in Eq. (1).

At the $\mu^+\mu^+$ collider, the doubly-charged scalar $\Delta_R^{\pm\pm}$ can lead to the process $\mu^+\mu^+ \rightarrow \ell^+\ell^+$ for $\ell = e, \mu$, as depicted in Fig. 1(d) and Fig. 1(e). For $m_{\Delta_R^{++}} < 2$ TeV, the signal process $\mu^+\mu^+ \rightarrow \gamma\Delta_R^{++}(\rightarrow \ell^+\ell^+)$ can also occur. The associated production of γ and Δ_R^{++} is displayed in Fig. 1(f) and Fig. 1(g), the latter of which involves the Yukawa interaction of Δ_R^{++} .

On the other hand, the μ^+e^- collider, which has been extensively utilized to search for CLFV signals, can also probe LNV through t -channel exchange of $\Delta_R^{\pm\pm}$ in the process $\mu^+e^- \rightarrow \mu^-e^+$, see Fig. 1(h). In the following, we will investigate the sensitivities to the Yukawa couplings f_R^{ee} and $f_R^{\mu\mu}$ in these processes.

Different from $\mu^+\mu^- \rightarrow \mu^+\mu^-$, the process $\mu^+\mu^+ \rightarrow \ell^+\ell^+$ receives contributions from $\Delta_R^{\pm\pm}$ via the s -channel, while SM γ/Z exchange occurs in the t -channel. Using the notation of Eq. (14) with $i = \mu^+\mu^+ \rightarrow \mu^+\mu^+$, the

NP contribution from doubly-charged scalar is given by

$$\sigma_{\mu^+\mu^+\rightarrow\mu^+\mu^+}^{\text{NP}} = [\sigma_{\Delta}(t) + \sigma_{\text{int}}(t)]|_{t_{\min}}^{t_{\max}}, \quad (26)$$

while the expression of SM cross section is lengthy and omitted. In the above,

$$\sigma_{\Delta}(t) = \frac{(f_R^{\mu\mu})^4}{64\pi} \frac{t}{|D_{\Delta}(s)|^2}, \quad (27)$$

$$\begin{aligned} \sigma_{\text{int}}(t) = & \frac{(f_R^{\mu\mu})^2 \alpha_{\text{em}}}{4} \frac{s - m_{\Delta^{++}}^2}{(s - m_{\Delta^{++}}^2)^2 + m_{\Delta^{++}}^2 \Gamma_{\Delta}^2} \ln \frac{s+t}{t} \\ & - \kappa_1 \tan^{-1} \frac{m_Z \Gamma_Z (s+2t)}{(m_Z^2 + s+t)(m_Z^2 - t) + m_Z^2 \Gamma_Z^2} \\ & + \kappa_2 \ln \frac{(s+t+m_Z^2)^2 + m_Z^2 \Gamma_Z^2}{(t-m_Z^2)^2 + m_Z^2 \Gamma_Z^2}, \end{aligned} \quad (28)$$

where $D_{\Delta}(s) \equiv s - m_{\Delta^{++}}^2 + i\Gamma_{\Delta} m_{\Delta^{++}}$, and we have introduced the definitions

$$\kappa_1 = \frac{(f_R^{\mu\mu})^2 \alpha_{\text{em}}}{64c_W^2 s_W^2} \frac{m_{\Delta^{++}} \Gamma_{\Delta}}{|D_{\Delta}(s)|^2}, \quad (29)$$

$$\kappa_2 = \frac{(f_R^{\mu\mu})^2 \alpha_{\text{em}}}{128c_W^2 s_W^2} \frac{s - m_{\Delta^{++}}^2}{|D_{\Delta}(s)|^2}. \quad (30)$$

In the above, the minimal and maximal values of t are defined as Eq. (21). The infrared divergence appearing in σ_{int} for the Mandelstam variable $t \rightarrow 0$ or $t \rightarrow -s$ is regularized after imposing the pseudo-rapidity cut as that for the Bhabha scattering. The relation between t and the pseudo-rapidity η is given in Eq. (20). We require $|\eta| < 2.5$, and obtain the cross section as depicted in Fig. 2.

For the process $\mu^+\mu^+ \rightarrow e^+e^+$, the cross section from the s -channel exchange of Δ_R^{++} is given by

$$\sigma_{\mu^+\mu^+\rightarrow e^+e^+} = \frac{(f_R^{ee})^2 (f_R^{\mu\mu})^2}{128\pi} \frac{s}{|D_{\Delta}(s)|^2}. \quad (31)$$

Note that there is no SM contribution to this process, so that its cross section is several orders of magnitude smaller than that of $\mu^+\mu^+ \rightarrow \mu^+\mu^+$, as illustrated in Fig. 2.

The doubly-charged scalar can also be produced in association with a photon $\mu^+\mu^+ \rightarrow \gamma\Delta_R^{++}$, if the center-of-mass energy $\sqrt{s} > m_{\Delta^{++}}$. The decay $\Delta_R^{++} \rightarrow \ell^+\ell^+$ for $\ell = e, \mu$ occurs subsequently. The cross section for the associated production is

$$\sigma_{\mu^+\mu^+\rightarrow\gamma\Delta_R^{++}} = \frac{e^2 (f_R^{\mu\mu})^2}{128\pi s^2} \sigma_{\gamma\Delta}(t)|_{t_{\min}}^{t_{\max}}, \quad (32)$$

where

$$\begin{aligned} \sigma_{\gamma\Delta}(t) = & \frac{(s^2 + m_{\Delta^{++}}^4) \ln(s - m_{\Delta^{++}}^2 + t)}{s - m_{\Delta^{++}}^2} - 4t \\ & - \frac{(5s^2 - 4m_{\Delta^{++}}^2 s + m_{\Delta^{++}}^4) \ln t}{s - m_{\Delta^{++}}^2}. \end{aligned} \quad (33)$$

The Mandelstam variable t for this process is defined as

$$t = -\frac{s - m_{\Delta^{++}}^2}{1 + e^{2\eta}}, \quad (34)$$

where η denotes the pseudo-rapidity of the photon, and the minimal and maximal values of t are given by

$$t_{\min} = -\frac{s - m_{\Delta^{++}}^2}{1 + e^{-2\eta_m}} \quad t_{\max} = -\frac{s - m_{\Delta^{++}}^2}{1 + e^{2\eta_m}}. \quad (35)$$

In the analysis, we impose the cut on photon $|\eta| < \eta_m = 2.5$. From Fig. 2, we can see that the cross section for $\mu^+\mu^+ \rightarrow \gamma\Delta_R^{++}$ increases with $m_{\Delta^{++}}$.

At the μ^+e^- collider, the process $\mu^+e^- \rightarrow \mu^-e^+$ can occur via t -channel exchange of $\Delta_R^{\pm\pm}$, which violates the lepton flavor number by two units $\Delta L_\mu = -\Delta L_e = 2$. The cross section is given by

$$\sigma_{\mu^+e^- \rightarrow \mu^-e^+} = \frac{(f_R^{ee})^2 (f_R^{\mu\mu})^2}{128\pi s^2} \left[s \frac{(s + 2m_{\Delta^{++}}^2)}{s + m_{\Delta^{++}}^2} - 2m_{\Delta^{++}}^2 \ln \frac{s + m_{\Delta^{++}}^2}{m_{\Delta^{++}}^2} \right]. \quad (36)$$

Since the flavor off-diagonal Yukawa couplings $f_R^{\alpha\beta}$ are smaller than the diagonal ones in order to satisfy the severe CLFV constraints, the contributions from the flavor off-diagonal couplings are not included. The cross section $\sigma_{\mu^+e^- \rightarrow \mu^-e^+}$ decreases with increasing $m_{\Delta^{++}}$, which is illustrated as the orange curve in Fig. 2.

Similar to the analyses at future MuC, we evaluate the sensitivities of the processes depending on whether they have SM contributions. For the process $\mu^+\mu^+ \rightarrow \mu^+\mu^+$, which can occur in the SM, we employ the statistical criterion of Eq. (22). For the processes $\mu^+e^- \rightarrow \mu^-e^+$, $\mu^+\mu^+ \rightarrow e^+e^+$ and $\mu^+\mu^+ \rightarrow \gamma\Delta_R^{++} (\rightarrow \ell^+\ell^+)$, which are purely beyond the SM, we require a minimum of three signal events, assuming negligible SM background. The resulting expected 95% CL exclusion limits are presented in Fig. 3 and Fig. 4.

V. RESULTS AND DISCUSSIONS

In this section, we discuss the combined constraints on the Yukawa couplings f_R^{ee} and $f_R^{\mu\mu}$ from the low-energy observables and high-energy processes. Two benchmark masses of the doubly-charged scalar, $m_{\Delta^{++}} = 1.4$ TeV and 3 TeV satisfying the LHC bound [65], are considered in Fig. 3 and Fig. 4, respectively. Processes at MuC and μ TRISTAN are labeled by their final states, which are given in parentheses. For the processes involving on-shell $\Delta_R^{\pm\pm}$ at colliders, we assume $f_R^{\tau\tau} = 0$ to derive its decay branching ratios.

Bhabha and Møller scattering are sensitive to f_R^{ee} . For $m_{\Delta^{++}} = 1.4$ TeV (3 TeV), LEP data [66] constrain the region $f_R^{ee} < 0.58$ (1.23), while the future MOLLER experiment [37] will be able to rule out $f_R^{ee} > 0.18$ (0.39). At CEPC/FCC-ee [69, 70], Bhabha scatter-

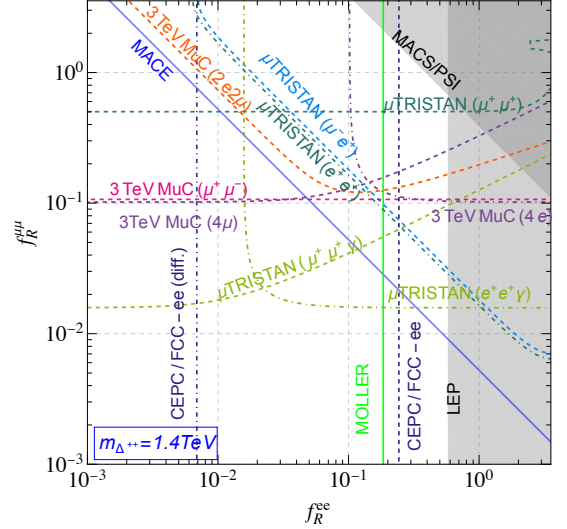


Figure 3: Current exclusion limits and future prospects of the Yukawa couplings f_R^{ee} and $f_R^{\mu\mu}$ for $m_{\Delta^{++}} = 1.4$ TeV. Gray regions indicate current 95% CL exclusion from measurements of $(g-2)_\mu$ [43, 44], Bhabha scattering at LEP [66], and searches for $M - \bar{M}$ transition at MACS/PSI [62]. Projected 95% CL sensitivity include those from future experiments: Bhabha scattering at CEPC/FCC-ee [69, 70], Møller scattering at MOLLER [37], $M - \bar{M}$ transition at MACE [55]. Also shown are prospects from high-energy analogues at a 3 TeV MuC [71, 72] and μ TRISTAN with $\mu^+\mu^+/\mu^+e^-$ beams [73], along with limits from direct pair and associated production processes at the MuC. The constraint from muon $g-2$ is too weak and not shown.

ing cross-section measurements can reach a sensitivity of $f_R^{ee} > 0.24$ (0.51). This can be significantly improved with differential cross-section measurements, testing values of f_R^{ee} as low as 0.007 (0.015).

Similarly, the processes $\mu^+\mu^- \rightarrow \mu^+\mu^-$ and $\mu^+\mu^+ \rightarrow \mu^+\mu^+$ are able to probe $f_R^{\mu\mu}$. For $m_{\Delta^{++}} = 1.4$ TeV (3 TeV), a 3 TeV MuC [71, 72] can test $f_R^{\mu\mu} > 0.1$ via precise measurements of $\mu^+\mu^- \rightarrow \mu^+\mu^-$, surpassing current limits from $(g-2)_\mu$ [43, 44]. This sensitivity, however, diminishes at a higher center-of-mass energy, $\sqrt{s} = 10$ TeV. Although $\mu^+\mu^+ \rightarrow \mu^+\mu^+$ at a 2 TeV μ TRISTAN has a larger cross section than $\mu^+\mu^- \rightarrow \mu^+\mu^-$ at a 3 TeV MuC (see Fig. 2), its expected constraint is weaker due to the assumed lower integrated luminosity of 12 fb^{-1} .

The $M - \bar{M}$ transition excludes the upper-right region in the $(f_R^{ee}, f_R^{\mu\mu})$ plane. In particular, MACS/PSI [62] has ruled out $f_R^{ee} f_R^{\mu\mu} > 0.39$ (1.78) for $m_{\Delta^{++}} = 1.4$ TeV (3 TeV). The lower limit can be extended by the future MACE experiment [55] to $f_R^{ee} f_R^{\mu\mu} > 3 \times 10^{-3}$ (2.4×10^{-2}). As a high-energy counterpart, $\mu^+e^- \rightarrow \mu^-e^+$ at μ TRISTAN is able to probe the region of $f_R^{ee} f_R^{\mu\mu} < 0.02$ (0.08), improving upon the MACS/PSI bounds by more

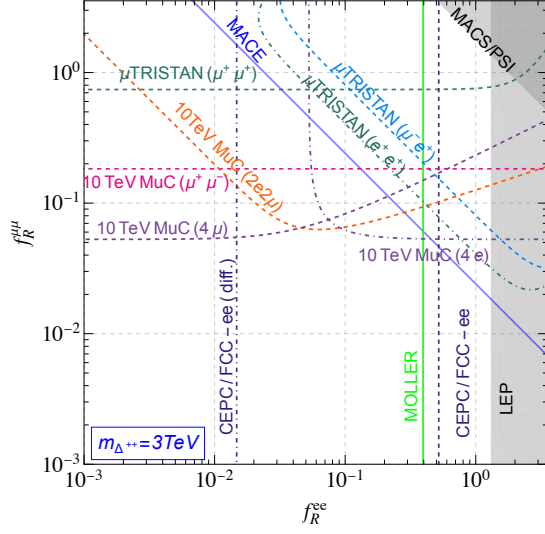


Figure 4: Same as Fig. 3, but for $m_{\Delta^{++}} = 3$ TeV and 10 TeV MuC.

than one order of magnitude.

Direct production of the doubly-charged scalar offers another avenue to simultaneously constrain f_R^{ee} and $f_R^{\mu\mu}$. At a MuC, the pair production $\mu^+\mu^- \rightarrow \Delta_R^{++}\Delta_R^{--}$ depends on $f_R^{\mu\mu}$, while the decay branching ratios of $\Delta_R^{\pm\pm} \rightarrow e^\pm e^\pm, \mu^\pm \mu^\pm$ vary with f_R^{ee} and $f_R^{\mu\mu}$. We find that $\mu^+\mu^- \rightarrow \Delta_R^{++}\Delta_R^{--} \rightarrow 4e$ is highly sensitive to both couplings. For $m_{\Delta_R^{++}} = 1.4$ TeV (3 TeV) at a 3 TeV (10 TeV) MuC, this channel can exclude much of the parameter space where $f_R^{ee}, f_R^{\mu\mu} > 0.1$ (0.05). In comparison, $\mu^+\mu^- \rightarrow \Delta_R^{++}\Delta_R^{--} \rightarrow 4\mu$ tests $f_R^{\mu\mu}$ down to 0.1 (0.05) when $f_R^{ee} < 0.05$; for larger f_R^{ee} , sensitivity to $f_R^{\mu\mu}$ drops quickly. The process $\mu^+\mu^- \rightarrow \Delta_R^{++}\Delta_R^{--} \rightarrow 2e2\mu$ exhibits a turnover in sensitivity: it increases with f_R^{ee} up to about 0.1 (0.04), beyond which it declines.

A similar finding holds for the associated production at μ TRISTAN. The channel $\mu^+\mu^+ \rightarrow \gamma\Delta_R^{++}(\rightarrow e^+e^+)$ is highly sensitive to both couplings, excluding most of the region where $f_R^{ee}, f_R^{\mu\mu} > 0.018$ for $m_{\Delta_R^{++}} = 1.4$ TeV. Meanwhile, $\mu^+\mu^+ \rightarrow \gamma\Delta_R^{++}(\rightarrow \mu^+\mu^+)$ can test $f_R^{\mu\mu}$ down to 0.018 if $f_R^{ee} < 6 \times 10^{-3}$, with sensitivity decreasing for larger f_R^{ee} . Since the center-of-mass energy of μ TRISTAN with $\mu^+\mu^+$ beams is 2 TeV, the associated production process is not applicable for $m_{\Delta_R^{++}} = 3$ TeV.

Besides, the process $\mu^+\mu^+ \rightarrow e^+e^+$, mediated by an off-shell Δ_R^{++} at μ TRISTAN, probes the product of the two Yukawa couplings. Its sensitivity relative to $\mu^+e^- \rightarrow \mu^-e^+$ at μ TRISTAN depends crucially on the mass of $\Delta_R^{\pm\pm}$. For $m_{\Delta_R^{++}} = 1.4$ TeV, $\mu^+e^- \rightarrow \mu^-e^+$ provides a comparable expected exclusion, while $\mu^+\mu^+ \rightarrow e^+e^+$ becomes superior for $m_{\Delta_R^{++}} = 3$ TeV.

Thus far, we have assumed $f_R^{\tau\tau} = 0$. Introducing a non-zero value leaves the sensitivities of low-energy probes and high-energy precision measurements in Fig. 1

(a), (b), (d), (e), and (h) unchanged. In contrast, the reach of direct production processes at MuC and μ TRISTAN in Fig. 1 (c), (f), (g) is diminished, as a non-zero $f_R^{\tau\tau}$ reduces the decay branching ratios of $\Delta_R^{\pm\pm}$ into electrons and muons.

VI. CONCLUSION

In this work, we have investigated the phenomenology of a TeV-scale doubly-charged scalar in various low-energy and high-energy experiments. Such a doubly-charged scalar arises naturally from the left-right symmetric model with D -parity breaking. Even with the stringent constraints from charged lepton flavor violation searches, the flavor-diagonal couplings of the right-handed doubly-charged scalar $\Delta_R^{\pm\pm}$ to leptons can be sizable.

We focus on the region of Yukawa couplings $f_R^{ee}, f_R^{\mu\mu} \gtrsim 10^{-3}$ for the mass of doubly-charged scalar being around $\mathcal{O}(1)$ TeV. Once being observed, it would provide compelling indirect evidence for the type-I seesaw mechanism as the origin of neutrino masses.

We study the contributions of $\Delta_R^{\pm\pm}$ to the low-energy observables, including the parity-violation asymmetry in Møller scattering, muon $g-2$, and muonium-antimuonium transition probability, and provide the full analytical expressions for the cross sections of the processes involving the doubly-charged scalar $\Delta_R^{\pm\pm}$ at future lepton colliders (cf. Fig. 1).

We derive constraints on the couplings f_R^{ee} and $f_R^{\mu\mu}$ for $m_{\Delta_R^{++}} = 1.4$ TeV and 3 TeV by analyzing both low- and high-energy probes at their projected sensitivities, as shown in Fig. 3 and Fig. 4, respectively. Our results show that future measurements of the parity-violating asymmetry in Møller scattering (MOLLER experiment) and searches for $M - \bar{M}$ transition (MACE experiment) can significantly extend the current bounds on the Yukawa couplings f_R^{ee} and $f_R^{\mu\mu}$. Furthermore, high-energy lepton colliders could probe coupling regions of $f_R^{ee} \gtrsim 10^{-1}$ and $f_R^{\mu\mu} \gtrsim 10^{-2}$ using the total cross sections. Sensitivity to f_R^{ee} could be improved to the level of $\sim 10^{-2}$ by analyzing the differential distribution of Bhabha scattering at CEPC/FCC-ee.

ACKNOWLEDGMENTS

We would like to thank Jian Tang and Yongchao Zhang for helpful discussions. GL is supported by the National Science Foundation of China under Grants No. 12347105 and No. 12505127, and the Guangdong Basic and Applied Basic Research Foundation (2024A1515012668). Jin Sun is supported by IBS under the project code, IBS-R018-D1.

-
- [1] P. Minkowski, *Phys. Lett. B* **67**, 421 (1977).
- [2] T. Yanagida, *Conf. Proc. C* **7902131**, 95 (1979).
- [3] M. Gell-Mann, P. Ramond, and R. Slansky, *Conf. Proc. C* **790927**, 315 (1979), [arXiv:1306.4669 \[hep-th\]](#).
- [4] R. N. Mohapatra and G. Senjanovic, *Phys. Rev. Lett.* **44**, 912 (1980).
- [5] S. L. Glashow, *NATO Sci. Ser. B* **61**, 687 (1980).
- [6] W. Konetschny and W. Kummer, *Phys. Lett. B* **70**, 433 (1977).
- [7] M. Magg and C. Wetterich, *Phys. Lett. B* **94**, 61 (1980).
- [8] J. Schechter and J. W. F. Valle, *Phys. Rev. D* **22**, 2227 (1980).
- [9] R. N. Mohapatra and G. Senjanovic, *Phys. Rev. D* **23**, 165 (1981).
- [10] T. P. Cheng and L.-F. Li, *Phys. Rev. D* **22**, 2860 (1980).
- [11] J. C. Pati and A. Salam, *Phys. Rev. D* **10**, 275 (1974), [Erratum: *Phys. Rev. D* **11**, 703–703 (1975)].
- [12] R. N. Mohapatra and J. C. Pati, *Phys. Rev. D* **11**, 2558 (1975).
- [13] R. N. Mohapatra and J. C. Pati, *Phys. Rev. D* **11**, 566 (1975).
- [14] G. Senjanovic and R. N. Mohapatra, *Phys. Rev. D* **12**, 1502 (1975).
- [15] G. Senjanovic, *Nucl. Phys. B* **153**, 334 (1979).
- [16] A. Zee, *Nucl. Phys. B* **264**, 99 (1986).
- [17] K. S. Babu, *Phys. Lett. B* **203**, 132 (1988).
- [18] K. S. Babu, S. Nandi, and Z. Tavartkiladze, *Phys. Rev. D* **80**, 071702 (2009), [arXiv:0905.2710 \[hep-ph\]](#).
- [19] F. Bonnet, D. Hernandez, T. Ota, and W. Winter, *JHEP* **10**, 076 (2009), [arXiv:0907.3143 \[hep-ph\]](#).
- [20] S. P. Das, F. F. Deppisch, O. Kittel, and J. W. F. Valle, *Phys. Rev. D* **86**, 055006 (2012), [arXiv:1206.0256 \[hep-ph\]](#).
- [21] J. Barry and W. Rodejohann, *JHEP* **09**, 153 (2013), [arXiv:1303.6324 \[hep-ph\]](#).
- [22] S. Davidson, B. Echenard, R. H. Bernstein, J. Heeck, and D. G. Hitlin, (2022), [arXiv:2209.00142 \[hep-ex\]](#).
- [23] D. Chang, R. N. Mohapatra, and M. K. Parida, *Phys. Rev. Lett.* **52**, 1072 (1984).
- [24] D. Chang, R. N. Mohapatra, and M. K. Parida, *Phys. Rev. D* **30**, 1052 (1984).
- [25] N. Sahu and U. Sarkar, *Phys. Rev. D* **74**, 093002 (2006), [arXiv:hep-ph/0605007](#).
- [26] F. F. Deppisch, T. E. Gonzalo, S. Patra, N. Sahu, and U. Sarkar, *Phys. Rev. D* **91**, 015018 (2015), [arXiv:1410.6427 \[hep-ph\]](#).
- [27] P. S. B. Dev, M. J. Ramsey-Musolf, and Y. Zhang, *Phys. Rev. D* **98**, 055013 (2018), [arXiv:1806.08499 \[hep-ph\]](#).
- [28] G. Li, M. J. Ramsey-Musolf, S. Urrutia Quiroga, and J. C. Vasquez, (2024), [arXiv:2408.06306 \[hep-ph\]](#).
- [29] E. Akhmedov, P. S. B. Dev, S. Jana, and R. N. Mohapatra, *Phys. Lett. B* **852**, 138616 (2024), [arXiv:2401.15145 \[hep-ph\]](#).
- [30] A. Crivellin, M. Ghezzi, L. Panizzi, G. M. Pruna, and A. Signer, *Phys. Rev. D* **99**, 035004 (2019), [arXiv:1807.10224 \[hep-ph\]](#).
- [31] P. S. B. Dev, B. Dutta, T. Ghosh, T. Han, H. Qin, and Y. Zhang, *JHEP* **03**, 068 (2022), [arXiv:2109.04490 \[hep-ph\]](#).
- [32] Y. Zhang, H. An, X. Ji, and R. N. Mohapatra, *Nucl. Phys. B* **802**, 247 (2008), [arXiv:0712.4218 \[hep-ph\]](#).
- [33] S. Bertolini, A. Maiezza, and F. Nesti, *Phys. Rev. D* **89**, 095028 (2014), [arXiv:1403.7112 \[hep-ph\]](#).
- [34] S. Bertolini, A. Maiezza, and F. Nesti, *Phys. Rev. D* **101**, 035036 (2020), [arXiv:1911.09472 \[hep-ph\]](#).
- [35] W. Dekens, L. Andreoli, J. de Vries, E. Mereghetti, and F. Oosterhof, *JHEP* **11**, 127 (2021), [arXiv:2107.10852 \[hep-ph\]](#).
- [36] T. G. Rizzo, *Phys. Rev. D* **25**, 1355 (1982), [Addendum: *Phys. Rev. D* **27**, 657–659 (1983)].
- [37] J. Benesch *et al.* (MOLLER), (2014), [arXiv:1411.4088 \[nucl-ex\]](#).
- [38] J. P. Leveille, *Nucl. Phys. B* **137**, 63 (1978).
- [39] J. F. Guion, J. Grifols, A. Mendez, B. Kayser, and F. I. Olness, *Phys. Rev. D* **40**, 1546 (1989).
- [40] A. Abada, C. Biggio, F. Bonnet, M. B. Gavela, and T. Hambye, *JHEP* **12**, 061 (2007), [arXiv:0707.4058 \[hep-ph\]](#).
- [41] Y. Cheng, X.-G. He, and J. Sun, *Phys. Lett. B* **827**, 136989 (2022), [arXiv:2112.09920 \[hep-ph\]](#).
- [42] F. Huang and J. Sun, *Phys. Rev. D* **110**, 115047 (2024), [arXiv:2409.13249 \[hep-ph\]](#).
- [43] D. P. Aguillard *et al.* (Muon $g-2$), (2025), [arXiv:2506.03069 \[hep-ex\]](#).
- [44] R. Aliberti *et al.*, (2025), [arXiv:2505.21476 \[hep-ph\]](#).
- [45] L. Morel, Z. Yao, P. Cladé, and S. Guellati-Khélifa, *Nature* **588**, 61 (2020).
- [46] R. H. Parker, C. Yu, W. Zhong, B. Estey, and H. Müller, *Science* **360**, 191 (2018), [arXiv:1812.04130 \[physics.atom-ph\]](#).
- [47] G. Gabrielse and G. Venanzoni, (2025), [arXiv:2507.11268 \[hep-ex\]](#).
- [48] R. Conlin and A. A. Petrov, *Phys. Rev. D* **102**, 095001 (2020), [arXiv:2005.10276 \[hep-ph\]](#).
- [49] C. Han, D. Huang, J. Tang, and Y. Zhang, *Phys. Rev. D* **103**, 055023 (2021), [arXiv:2102.00758 \[hep-ph\]](#).
- [50] T. Fukuyama, Y. Mimura, and Y. Uesaka, *Phys. Rev. D* **105**, 015026 (2022), [arXiv:2108.10736 \[hep-ph\]](#).
- [51] T. Fukuyama, Y. Mimura, and Y. Uesaka, *Phys. Rev. D* **106**, 055041 (2022), [Erratum: *Phys. Rev. D* **107**, 079903 (2023)], [arXiv:2206.09691 \[hep-ph\]](#).
- [52] T. Fukuyama, Y. Mimura, and Y. Uesaka, *Phys. Rev. D* **108**, 095029 (2023), [arXiv:2309.02060 \[hep-ph\]](#).
- [53] M. Ghosh, K. Liguori, T. Okui, and K. Tobioka, (2025), [arXiv:2504.05378 \[hep-ph\]](#).
- [54] A.-Y. Bai *et al.*, in *Snowmass 2021* (2022) [arXiv:2203.11406 \[hep-ph\]](#).
- [55] A.-Y. Bai *et al.*, (2024), [arXiv:2410.18817 \[hep-ex\]](#).
- [56] N. Kawamura, R. Kitamura, H. Yasuda, M. Otani, Y. Nakazawa, H. Inuma, and T. Mibe, *JPS Conf. Proc.* **33**, 011120 (2021).
- [57] G. Feinberg and S. Weinberg, *Phys. Rev.* **123**, 1439 (1961).
- [58] J. Heeck and M. Sokhashvili, *Phys. Lett. B* **852**, 138621 (2024), [arXiv:2401.09580 \[hep-ph\]](#).
- [59] D. Chang and W.-Y. Keung, *Phys. Rev. Lett.* **62**, 2583 (1989).
- [60] M. L. Swartz, *Phys. Rev. D* **40**, 1521 (1989).
- [61] G. Cvetic, C. O. Dib, C. S. Kim, and J. D. Kim, *Phys. Rev. D* **71**, 113013 (2005), [arXiv:hep-ph/0504126](#).
- [62] L. Willmann *et al.*, *Phys. Rev. Lett.* **82**, 49 (1999), [arXiv:hep-ex/9807011](#).

- [63] K. Horikawa and K. Sasaki, *Phys. Rev. D* **53**, 560 (1996), [arXiv:hep-ph/9504218](#).
- [64] W.-S. Hou and G.-G. Wong, *Phys. Lett. B* **357**, 145 (1995), [arXiv:hep-ph/9505300](#).
- [65] G. Aad *et al.* (ATLAS), *Eur. Phys. J. C* **83**, 605 (2023), [arXiv:2211.07505 \[hep-ex\]](#).
- [66] S. Schael *et al.* (ALEPH, DELPHI, L3, OPAL, LEP Electroweak), *Phys. Rept.* **532**, 119 (2013), [arXiv:1302.3415 \[hep-ex\]](#).
- [67] J. Abdallah *et al.* (DELPHI), *Eur. Phys. J. C* **45**, 589 (2006), [arXiv:hep-ex/0512012](#).
- [68] T. Nomura, H. Okada, and H. Yokoya, *Nucl. Phys. B* **929**, 193 (2018), [arXiv:1702.03396 \[hep-ph\]](#).
- [69] M. Dong *et al.* (CEPC Study Group), (2018), [arXiv:1811.10545 \[hep-ex\]](#).
- [70] A. Abada *et al.* (FCC), *Eur. Phys. J. ST* **228**, 261 (2019).
- [71] D. Stratakis *et al.* (Muon Collider), (2022), [arXiv:2203.08033 \[physics.acc-ph\]](#).
- [72] C. Accettura *et al.* (International Muon Collider), *CERN Yellow Rep. Monogr.* **2/2024**, 176 (2024), [arXiv:2407.12450 \[physics.acc-ph\]](#).
- [73] Y. Hamada, R. Kitano, R. Matsudo, H. Takaura, and M. Yoshida, *PTEP* **2022**, 053B02 (2022), [arXiv:2201.06664 \[hep-ph\]](#).
- [74] Y. Hamada, R. Kitano, R. Matsudo, and H. Takaura, *PTEP* **2023**, 013B07 (2023), [arXiv:2210.11083 \[hep-ph\]](#).
- [75] J. Alwall, R. Frederix, S. Frixione, V. Hirschi, F. Maltoni, O. Mattelaer, H. S. Shao, T. Stelzer, P. Torrielli, and M. Zaro, *JHEP* **07**, 079 (2014), [arXiv:1405.0301 \[hep-ph\]](#).
- [76] R. Frederix, S. Frixione, V. Hirschi, D. Pagani, H. S. Shao, and M. Zaro, *JHEP* **07**, 185 (2018), [Erratum: *JHEP* **11**, 085 (2021)], [arXiv:1804.10017 \[hep-ph\]](#).
- [77] X. Sun, “Lumical design in CEPC,” <https://indico.ihep.ac.cn/event/26108/contributions/189916/attachments/90729/118020/Lumical.pdf> (2025), nanjing University, Accessed: 2025-10-2.
- [78] M. Belfkir, T. A. Chowdhury, and S. Nasri, *Phys. Lett. B* **852**, 138605 (2024), [arXiv:2307.16111 \[hep-ph\]](#).
- [79] T. Junk, *Nucl. Instrum. Meth. A* **434**, 435 (1999), [arXiv:hep-ex/9902006](#).
- [80] P. N. Bhattiprolu, S. P. Martin, and J. D. Wells, *Eur. Phys. J. C* **81**, 123 (2021), [arXiv:2009.07249 \[physics.data-an\]](#).
- [81] M. Abe *et al.*, *PTEP* **2019**, 053C02 (2019), [arXiv:1901.03047 \[physics.ins-det\]](#).